Near-Unity Cooper Pair Splitting Efficiency

J. Schindele, A. Baumgartner,* and C. Schönenberger

Department of Physics, University of Basel, Klingelbergstrasse 82, CH-4056 Basel, Switzerland

The two electrons of a Cooper pair in a conventional superconductor form a spin singlet and therefore a maximally entangled state. Recently, it was demonstrated that the two particles can be extracted from the superconductor into two spatially separated contacts via two quantum dots in a process called Cooper pair splitting (CPS). Competing transport processes, however, limit the efficiency of this process. Here we demonstrate efficiencies up to 90%, significantly larger than required to demonstrate interaction-dominated CPS, and on the right order to test Bell's inequality with electrons. We compare the CPS currents through both quantum dots, for which large apparent discrepancies are possible. The latter we explain intuitively and in a semiclassical master equation model. Large efficiencies are required to detect electron entanglement and for prospective electronics-based quantum information technologies.

PACS numbers: 74.45.+c, 03.67.Bg, 73.23.−b, 73.63.Nm

Quantum entanglement between two particles is a fundamental resource for quantum information technologies [1]. Experiments with entangled photons are well developed and already offer first applications [2]. However, entanglement between electrons, the fundamental particles of electronics, is difficult to create in a controlled way. Electron-electron interactions, for example in the Fermi sea of a metal, tend to destroy particle correlations. In contrast, in nanostructured electronic devices, interactions can be exploited, for example to generate entangled photons [3].

In a conventional superconductor the electrons form spin singlet Cooper pairs in the BCS ground state. If such pairs can be extracted coherently, they can in principle serve as a source of spatially separated entangled electrons [4,5]. The process of converting a Cooper pair into two electrons in different normal metal contacts is called crossed Andreev reflection or Cooper pair splitting (CPS) and can lead to electronic correlations in metallic samples [6–10]. CPS can be enforced and electrically tuned by coupling the superconductor to two quantum dots (QDs), which inhibits the simultaneous transport of two electrons into the same contact. Recently, CPS was demonstrated on devices with a superconductor S coupled to two parallel QDs, each with a normal metal output lead N1 and N2, as shown schematically in Fig. 1(a) [11–14]. In these experiments local (Cooper) pair tunneling (LPT, see below) and other competing processes reduced the CPS efficiency to a few percent up to 50%. Such values can in principle be reached without enforcing the splitting by electron-electron interactions on the QDs, e.g., in a chaotic cavity [15], or in a double-dot system with strong interdot coupling [12], where the electrons of a Cooper pair can exit the device through two ports at random. However, for applications and more sophisticated experiments, for example the explicit demonstration of entanglement, efficiencies close to unity are required.

Here we present CPS experiments on a carbon nanotube (CNT) device and demonstrate efficiencies up to 90%, values only possible with electron-electron interactions on the QDs. In addition, we find discrepancies between the CPS part of the currents through the two QDs, which we relate to a competition between local processes and CPS in a semiclassical master equation model. The large CPS efficiencies and the increased understanding of the relevant mechanisms are important steps on the way to an all-electronic source of entangled electron pairs in a solid-state device.

An artificially colored scanning electron micrograph of a CPS device is shown in Fig. 1(b), together with a schematic of the measurement. A CVD-grown CNT (arrow) is contacted in the center by a 200 nm wide palladium/aluminum (thicknesses 4 nm/60 nm) contact (S), which becomes superconducting below ∼1.1 K. Two pure Pd contacts to the right and left of S serve as normal metal contacts N1 and N2, both of which define a QD (QD1 and QD2) on the two CNT segments adjacent to S. The QDs can be tuned electrically by a global backgate and the local side gates SG1 and SG2.

The experiments are performed in a dilution refrigerator at a base temperature of ∼20 mK. From standard charge stability diagrams we extract charging energies of
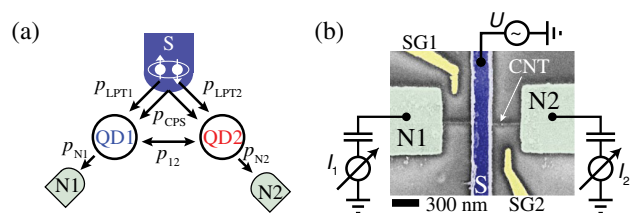

FIG. 1 (color online).   (a) Schematic of the device geometry. The probabilities for the individual transport processes, p_i, are discussed in the text. (b) Scanning electron micrograph of the CPS device and measurement setup.

~7 meV for QD1 and ~4 meV for QD2, an orbital energy spacing of ~1 meV, and an energy gap due to the superconductor of ~120 μeV. With S in the normal state we find typical level broadenings of ~150–500 μeV. Relatively low peak conductances suggest a rather asymmetric coupling of the QDs to the leads. The lever arms from a side gate across the superconductor to the other QD is roughly ten times smaller than that of a local side gate. In conductance measurements with the two QDs in series we do *not* observe an anticrossing of the QD resonances. This difference to Ref. [12] might be due to the larger width of S and allows us to tune both QDs individually through resonances without a hybridization of the QD levels.

Figures 2(a) and 2(b) show the simultaneously recorded differential conductances G_1 through QD1 and G_2 through QD2, both as a function of the side-gate voltages U_{SG1} and U_{SG2}. The measurements were done at zero bias and zero magnetic field. When U_{SG1} is varied, QD1 is tuned through several resonances, which result in conductance maxima in G_1, labeled L1, L2, and L3 in Fig. 2(a). The amplitudes of the resonances vary only little when tuning U_{SG2}, while the resonance positions change slightly due to capacitive cross talk from SG2 to QD1. Very weak, but similar conductance ridges labeled R1, R2, and R3 can be observed in the conductance through QD2 in Fig. 2(b). These are mainly tuned by SG2, which results in conductance ridges almost perpendicular to the ones in Fig. 2(a) due to QD1 [16].

Our main experimental findings are pronounced peaks when both QDs are in resonance. At these gate configurations the conductance is increased by up to a factor of ~100 compared to the respective conductance ridge. This is most prominent in G_2, but most of the peaks can also be observed in G_1 on a larger background. No peaks at resonance crossings can be observed when the

superconductivity is suppressed by a small external magnetic field (see below and Supplemental Material [17]). If only one QD is resonant, only local transport through this QD is allowed. A possible local process is LPT, illustrated in Fig. 2(c): the first electron of a Cooper pair is emitted into the QD, which leaves S in a virtual excited state. When the first electron has left the dot, the second tunnels into the same QD. Other local processes like double charging of a dot are strongly suppressed by the large charging energies. However, if both QDs are in resonance, the second electron can tunnel into QD2, as shown in Fig. 2(d), which splits the initial Cooper pair.

We now focus on the resonance crossing (L2, R2). Figure 3(a) shows the Coulomb blockade resonance L2 in G_1 as a function of U_{SG1} (bottom curve). In the same gate sweep, G_2 is tuned through the resonance R2 due to capacitive cross talk, which results in a wide conductance maximum. However, an additional much sharper peak occurs at the voltage of the L2 resonance, with similar width and shape as the resonance in G_1. When the superconductivity is suppressed by an external magnetic field of 250 mT, we find no additional peak in G_2 at the resonance crossing, but a slight reduction consistent with a classical resistor network [11] and a small capacitive coupling between the QDs, see inset of Fig. 3(a) and the Supplemental Material [17]. The
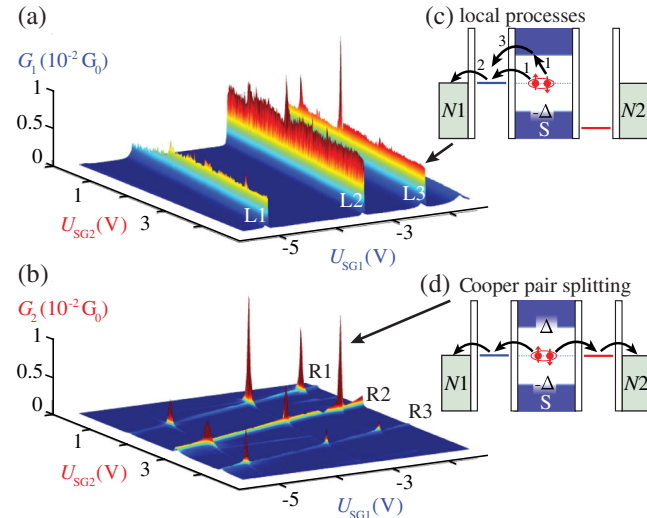

FIG. 2 (color online). (a) Differential conductance G_1 of QD1 and (b) G_2 of QD2 as a function of the side-gate voltages U_{SG1} and U_{SG2}. (c) and (d) Energy diagrams of local (Cooper) pair tunneling (LPT) and CPS.
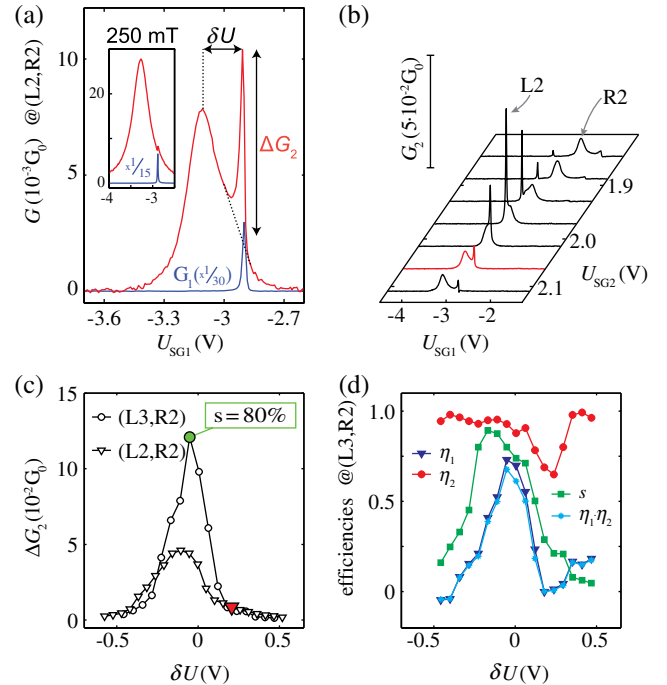

FIG. 3 (color online). (a) G_1 and G_2 as a function of U_{SG1} for $U_{SG2} \approx 2.07$ V. Inset: the same measurement at a magnetic field of 250 mT to suppress the superconductivity. (b) $G_2(U_{SG1})$ for a series of side-gate voltages U_{SG2}. (c) ΔG_2 as a function of the detuning δU between the resonances in QD1 and QD2 for the indicated resonance crossings. (d) Plots of the visibilities η_i, the CPS efficiency s and $\eta = \eta_1 \eta_2$.

resonance positions do not change with the field, but the overall conductance can vary strongly due to the superconductor's gap, which reduces local single electron transport.

As a measure for the CPS *rates* in the experiments we use the amplitude ΔG_2 of the additional peak in G_2 at the position of the QD1 resonance, as illustrated in Fig. 3(a). The subtracted background is determined by manually interpolating the bare QD2 resonance. δU is the detuning between the two resonances. Figure 3(b) shows a series of SG1 sweeps at different values of U_{SG2} near the resonance crossing (L2, R2), with the curve from Fig. 3(a) highlighted in red. One finds that ΔG_2 depends strongly on the detuning δU. In Fig. 3(c) we therefore plot ΔG_2 vs δU, where the value of Fig. 3(a) is marked by a red triangle. As another example, the conductance variation near the crossing (L3, R2) is also plotted in Fig. 3(c). For all crossings we find that ΔG_2 has a maximum at $\delta U \approx 0$, i.e., where both QDs are in resonance, in agreement with theoretical predictions [4]. For $\delta U \neq 0$, ΔG_2 falls off rapidly and tends to zero on an energy scale consistent with the width of the respective resonances.

On the resonance crossings investigated here, the maximum change in G_2 is $0.012 e^2/h$. This number has to be compared to the total conductance, including the local processes, so that we define the *visibility* of CPS in the second branch of the Cooper pair splitter as $\eta_2 = \Delta G_2/G_2$ (similar for G_1). The CPS visibilities for both branches on resonance crossing (L3, R2) are plotted in Fig. 3(d). η_2 is essentially constant over a large range of δU and reaches values up to 98%; i.e., the current in one branch can be dominated by CPS. η_1, however, has a maximum of only 73% at $\delta U \approx 0$ and drops to zero for a large detuning.

As a measure for the CPS *efficiency* we compare the CPS currents to the total currents in both branches of the device. Assuming that CPS leads to a conductance G_{CPS} in each branch, independent of other processes, we define the CPS efficiency as

$$s = \frac{2G_{CPS}}{G_1 + G_2}. \tag{1}$$

By assuming that $G_{CPS} = \Delta G_2$ we find efficiencies up to $s \approx 90\%$, much larger than required to demonstrate interaction induced CPS. The efficiency as a function of δU is plotted in Fig. 3(d) for the crossing (L3, R2). However, depending on the intended purpose of the entangler, s is not necessarily the relevant parameter. For example, in tests of Bell's inequality proposed for electrons [18,19], the measured quantities are current cross correlations between the normal metal terminals, which suggests using the following figure of merit:

$$\eta = \eta_1 \eta_2 = \frac{\Delta G_1}{G_1} \frac{\Delta G_2}{G_2}. \tag{2}$$

A violation of Bell's inequality requires $\eta > 1/\sqrt{2} \approx 71\%$. In Fig. 3(d), η is plotted as a function of δU for the crossing (L3, R2). We find values up to $\eta = 68\%$, mostly limited by

the large rates of local processes through QD1. Nonetheless, the large visibility in G_2 demonstrates the feasibility of testing Bell's inequality with electrons, if an ideal detection scheme was available.

Intuitively one might expect $\Delta G_1 = \Delta G_2$. This is found within experimental errors for 4 of the 9 resonance crossings. As an example, ΔG_1 and ΔG_2 of the crossing (L3, R2) investigated above are plotted as a function of δU in Fig. 4(a). For the other crossings, the two conductance variations deviate significantly from each other. Four of the 9 crossings exhibit curves comparable to (L3, R1) plotted in Fig. 4(b). Here, ΔG_2 is larger than ΔG_1 by about a factor of 2, but with a similar curve shape. One of the 9 crossings, (L2, R1) shown in Fig. 4(c), is very peculiar: the variation in ΔG_1 is almost negligible, while ΔG_2 exhibits a pronounced peak. In addition, one finds that $\Delta G_2 > G_1$; i.e., the conductance variation in one branch is larger than the total conductance in the other.

To qualitatively understand our experiments we discuss the electron dynamics in our devices using a strongly simplified semi-classical master equation model. Details can be found in the Supplemental Material [17] and more sophisticated models in Refs. [20,21]. For each QD we consider a single level with constant broadening and a large charging energy. The system can be in one of the following four states: both QDs empty, (0,0), either QD filled with one electron, (1,0) or (0,1), or both dots occupied, (1,1). The transport processes illustrated in Fig. 1(a) lead to transitions between these states [17]. For example, CPS changes the system from (0,0) to (1,1). The p_i in
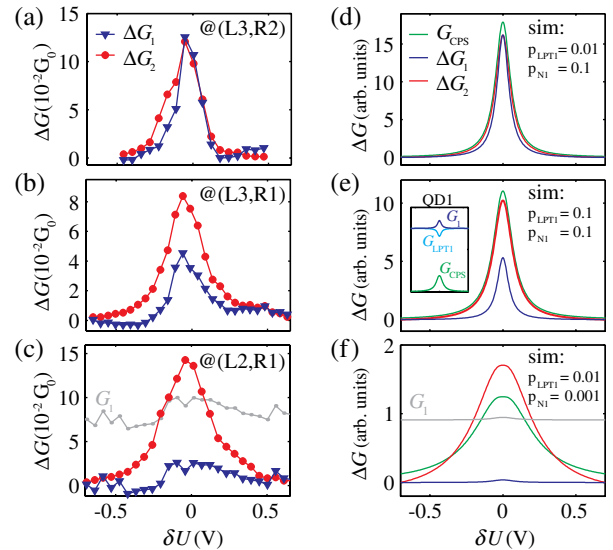

FIG. 4 (color online). (a)–(c) ΔG_1 and ΔG_2 as a function of the detuning δU for the indicated resonance crossings. (d)–(f) Similar plots obtained from the master equation model of CPS, including G_{CPS}. The parameters varied between the simulations are given in the figures. The inset in (e) shows the conductances in the branch of QD1 due to local processes (G_{LPT1}), CPS and at N1.

Fig. 1(a) denote the respective rates (with arbitrary units) of such a change of the system state occupation. Since the p_i are effective values that can depend in a nontrivial way on several tunnel barriers and the superconducting gap, we only assign rough values that qualitatively reproduce the experimental findings. In addition, we assume that electrons are transferred only in one direction, from S to the QDs and from the QDs to the respective normal metal contact. We also consider a tunnel coupling between the dots. The resonances are incorporated by gate-dependent Gaussian weights for p_{CPS}, p_{Ni} and p_{12} [17]. We use a diagrammatic method based on maximal trees to obtain the steady-state occupation probabilities from the corresponding master equation [22]. From the populations of the QDs we then calculate the transport rates [17].

Our model shows that a finite QD population can lead to a competition between the various transport mechanisms. In Figs. 4(d)–4(f), simulated conductance variations are plotted for different QD1 parameters, while those of QD2 are kept at $p_{LPT2} = 0.01$ and $p_{N2} = 0.1$ for all plots, i.e., in the regime of Ref. [4], where the coupling to S is much weaker than to the normal contacts. We set $p_{CPS} = 0.03$ to obtain conductances comparable to the experiments, and $p_{12} = 0.001$ so that the interdot coupling is the smallest parameter in the problem. If the occupation of both QDs are negligible, i.e., $p_{LPTi} \ll p_{Ni}$, one finds $\Delta G_1 = \Delta G_2$, as shown in Fig. 4(d) [23], similar to the experiments presented in Fig. 4(a).

If one QD occupation becomes significant, the conductance variations are not identical anymore. Figure 4(e) shows plots for $p_{LPT1} = p_{N1} = 0.1$, for which $\Delta G_2 \approx 2\Delta G_1$, as in the experiment shown in Fig. 4(b). The model also allows us to calculate the rate at which Cooper pairs are extracted from S by CPS. The corresponding conductance is also plotted in Figs. 4(d)–4(f). We find that $\Delta G_i < G_{CPS}$ as long as the interdot coupling p_{12} is negligible; i.e., the experimentally extracted CPS conductance underestimates the actual value, $\max(\Delta G_1, \Delta G_2) < G_{CPS}$. The explanation is that due to CPS on a resonance crossing the average QD populations are increased beyond the off-resonance equilibrium due to the local processes, which leads to a reduction of the local current into the N contacts. This is illustrated in the inset of Fig. 4(e), where the calculated local conductance from S to QD1, G_{LPT1}, has a minimum where G_{CPS} is maximal. Intuitively, the QDs are not emptied fast enough, which inhibits all processes on the dot. This suppression mechanism might account for the discrepancy between noise correlations and conductance measurements in Ref. [14].

The situation is more complex if the tunnel coupling between the dots becomes relevant. For example, if $p_{N1} = p_{12} = 0.001$ and $p_{LPT1} = 0.01 > p_{N1}$, as used for Fig. 4(f), the electrons can leave QD1 to N1 and to QD2 with the same probability. Since p_{N1} is small, this quenches G_1, but G_2 is increased due to the additional current from QD1. Here, the ΔG_i do not give an upper or lower bound

for the CPS rate and ΔG_2 can become larger than G_1, as in the experimental curves in Fig. 4(c). We note that the discussed situations are not in the regime of completely filled QDs. Our model suggests that in this unitary limit the conductances can be reduced considerably in the center of a resonance crossing, which might account for the as yet unexplained anomalous behavior of the on-resonance signals in Ref. [11].

In summary, we present CPS experiments with efficiencies up to 90%, demonstrating the importance of electron-electron interactions in such systems. For the figure of merit relevant in tests of Bell's inequality for electrons we find values close to the required limits. In addition, we asses CPS on both QDs and find rather large apparent discrepancies between the two conductance variations, which we explain in a semi-classical master equation model. The latter suggests that for negligible interdot couplings the experimentally extracted CPS rates are a lower bound to the real CPS rates. Our experiments and calculations show that there is a large variety of different transport phenomena in a Cooper pair splitter device that need further investigation. Of capital importance is the observation that if both dots had the properties of QD2, tests of Bell's inequality even with nonideal detectors could be performed to detect electron entanglement, an important step on the way to a source of entangled electron pairs on demand.

*andreas.baumgartner@unibas.ch

[1] G. Vidal, Phys. Rev. Lett. **91**, 147902 (2003).

[2] R. Ursin, F. Tiefenbacher, T. Schmitt-Manderbach, H. Weier, T. Scheidl, M. Lindenthal, B. Blauensteiner, T. Jennewein, J. Perdigues, P. Trojek, B. Ober, M. Fürst, M. Meyenburg, J. Rarity, Z. Sodnik, C. Barbieri, H. Weinfurter, and A. Zeilinger, Nature Phys. **3**, 481 (2007).

[3] C. L. Salter, R. M. Stevenson, I. Farrer, C. A. Nicoll, D. A. Ritchie, and A. J. Shields, Nature (London) **465**, 594 (2010).

[4] P. Recher, E. V. Sukhorukov, and D. Loss, Phys. Rev. B **63**, 165314 (2001).

[5] G. B. Lesovik, T. Martin, and G. Blatter, Eur. Phys. J. B **24**, 287 (2001).

[6] D. Beckmann, H. B. Weber, and H. v. Löhneysen, Phys. Rev. Lett. **93**, 197003 (2004).

[7] S. Russo, M. Kroug, T. M. Klapwijk, and A. F. Morpurgo, Phys. Rev. Lett. **95**, 027002 (2005).

[8] P. Cadden-Zimansky, J. Wei, and V. Chandrasekhar, Nature Phys. **5**, 393 (2009).

[9] A. Kleine, A. Baumgartner, J. Trbovic, and C. Schönenberger, Europhys. Lett. **87**, 27011 (2009).

[10] J. Wei and V. Chandrasekhar, Nature Phys. **6**, 494 (2010).

[11] L. Hofstetter, S. Csonka, J. Nygård, and C. Schönenberger, Nature (London) **461**, 960 (2009).

[12] L. G. Herrmann, F. Portier, P. Roche, A. L. Yeyati, T. Kontos, and C. Strunk, Phys. Rev. Lett. **104,** 026801 (2010).

[13] L. Hofstetter, S. Csonka, A. Baumgartner, G. Fülöp, S. d'Hollosy, J. Nygård, and C. Schönenberger, Phys. Rev. Lett. **107,** 136801 (2011).

[14] A. Das, Y. Ronen, M. Heiblum, D. Mahalu, A. V. Kretinin, and H. Shtrikman, arXiv:1205.2455v1.

[15] P. Samuelsson and M. Büttiker, Phys. Rev. B **66,** 201306 (2002).

[16] The two weak lines between $R1/R2$ and $R2/R3$ at two constant U_{SG1} values are probably due to random charge rearrangements.

[17] See Supplemental Material at http://link.aps.org/supplemental/10.1103/PhysRevLett.109.157002 for control measurements and model details.

[18] S. Kawabata, J. Phys. Soc. Jpn. **70,** 1210 (2001).

[19] P. Samuelsson, E. V. Sukhorukov, and M. Büttiker, Phys. Rev. Lett. **91,** 157002 (2003).

[20] O. Sauret, D. Feinberg, and T. Martin, Phys. Rev. B **70,** 245313 (2004).

[21] J. Eldridge, M. G. Pala, M. Governale, and J. König, Phys. Rev. B **82,** 184507 (2010).

[22] J. Schnakenberg, Rev. Mod. Phys. **48,** 571 (1976).

[23] For clarity we chose slightly different widths for the QD resonances.